Int. J. Radiation Oncology Biol. Phys., Vol. 57, No. 2, pp. 543–552, 2003

0360-3016/03/$–see front matter

ELSEVIER

doi:10.1016/S0360-3016(03)00499-1

BIOLOGY CONTRIBUTION

IMPACT OF PROLONGED FRACTION DELIVERY TIMES ON TUMOR CONTROL: A NOTE OF CAUTION FOR INTENSITY-MODULATED RADIATION THERAPY (IMRT)

JIAN Z. WANG, PH.D.,* X. ALLEN LI, PH.D.,* WARREN D. D'SOUZA, PH.D.,* AND ROBERT D. STEWART, PH.D.†

*Department of Radiation Oncology, University of Maryland School of Medicine, Baltimore, MD; †School of Health Sciences, Purdue University, West Lafayette, IN

Purpose: **Intensity-modulated radiation therapy (IMRT) allows greater dose conformity to the tumor target. However, IMRT, especially static delivery, usually requires more time to deliver a dose fraction than conventional external beam radiotherapy (EBRT). The purpose of this work is to explore the potential impact of such prolonged fraction delivery times on treatment outcome.**

Methods and Materials: **The generalized linear-quadratic (LQ) model, which accounts for sublethal damage repair and clonogen proliferation, was used to calculate the cell-killing efficiency of various simulated and clinical IMRT plans. LQ parameters derived from compiled clinical data for prostate cancer ($\alpha = 0.15$ Gy^{-1}, $\alpha/\beta = 3.1$ Gy, and a 16-min repair half-time) were used to compute changes in the equivalent uniform dose (EUD) and tumor control probability (TCP) due to prolonged delivery time of IMRT as compared with conventional EBRT. EUD and TCP calculations were also evaluated for a wide range of radiosensitivity parameters. The effects of fraction delivery times ranging from 0 to 45 min on cell killing were studied.**

Results: **Our calculations indicate that fraction delivery times in the range of 15–45 min may significantly decrease cell killing. For a prescription dose of 81 Gy in 1.8 Gy fractions, the EUD for prostate cancer decreases from 78 Gy for a conventional EBRT to 69 Gy for an IMRT with a fraction delivery time of 30 min. The values of EUD are sensitive to the α/β ratio, the repair half-time, and the fraction delivery time. The instantaneous dose-rate, beam-on time, number of leaf shapes (segments), and leaf-sequencing patterns given the same overall fraction delivery time were found to have negligible effect on cell killing.**

Conclusions: **The total time to deliver a single fraction may have a significant impact on IMRT treatment outcome for tumors with a low α/β ratio and a short repair half-time, such as prostate cancer. These effects, if confirmed by clinical studies, should be considered in designing IMRT treatments.** **© 2003 Elsevier Inc.**

IMRT, Fraction delivery time, Tumor-cell repair, Prostate cancer.

INTRODUCTION

Intensity-modulated radiation therapy (IMRT) is a technique of radiation delivery developed to improve target dose conformity and normal tissue sparing (1–4). IMRT delivers dose, either dynamically or statically (e.g., step-and-shoot), using many beam apertures (segments) that are shaped with multileaf collimator (MLC) (1, 4, 5). Whereas conventional external beam radiotherapy (EBRT) takes about 2–5 min to deliver a treatment fraction, IMRT with static delivery typically requires 15 to 45 min to deliver the same fractional dose. Cell killing tends to decrease with increasing fraction delivery time because of sublethal damage repair. To our knowledge, very few studies have been published to date that characterize the impact of IMRT delivery time on local tumor control (e.g., 6–8). Calculations using biologic models show that, for a decrease in dose-rate from 1 to 0.1 Gy/min, the biologically effective dose (BED) to the tumor may be reduced by 10% or more (6–8). Very recently, Morgan *et al.* (9) have conducted an *in vitro* experiment to explore the impact of fraction delivery time on cell survival. They reported that the cell-surviving fraction for a fraction delivery time of 20 min was significantly higher than that for 2–6 min. More detailed and systematic studies on the impact of the prolonged IMRT delivery time are required.

The linear-quadratic (LQ) model has been widely used to describe cell killing for radiation therapy applications. The quadratic term in the LQ model reflects a cell's capability to repair sublethal damage. When fraction delivery times are

Reprint requests to: X. Allen Li, Ph.D., Department of Radiation Oncology, University of Maryland, 22 South Greene Street, Baltimore, MD 21201-1595. Tel: (410) 328-7165; Fax: (410) 328-2618; E-mail: ali001@umaryland.edu

Acknowledgments—The authors would like to thank Drs. William F. Morgan and M. Guerrero of the University of Maryland for their valuable inputs on this study.

Received Oct 29, 2002, and in revised form Apr 2, 2003. Accepted for publication Apr 11, 2003.

comparable to or longer than the half-time for repair, decreases in cell killing due to sublethal damage repair may significantly reduce overall treatment effectiveness. For human tumor cells, the characteristic repair half-time ranges from a few minutes to several hours (10–12). In a review article, Steel *et al.* (10) pointed out that the repair time for many tumors appears different when measured from a split-dose experiment vs. a low-dose-rate (LDR) exposure. They attributed this difference to the presence of two or more repair components. Others have confirmed that nonexponential or multi-exponential sublethal damage repair kinetics are involved in cell killing (13–17). In split-dose survival experiments, the fast and slow rates of sublethal damage repair kinetics can be reasonably approximated by a single (average) first-order repair term. In LDR experiments, cell killing is more sensitive to the fast repair component. For fraction delivery times in the range of 15 to 45 min (i.e., comparable to IMRT treatment times), the fast repair component is important, and the slow repair component usually has little impact on cell killing. Brenner and Hall (11) have compiled *in vitro* data on the repair half-times of human cancer cell lines under LDR exposure conditions. They have found that the most probable repair half-time is approximately 20 min. For prostate cancer, Wang *et al.* (18) used clinical data to derive a repair half-time of 16 min with a standard (68%) confidence interval from 0 to 90 min. Repair half-times such as these are comparable to the fraction delivery times typically found in IMRT. Consequently, cell killing may be affected by fraction delivery times found in some IMRT treatment plans.

In the LQ formalism, dose rate effects are included by applying a so-called dose protraction factor to the quadratic term (i.e. βD^2). This dose protraction factor G depends on the characteristic repair rate of sublethal damage. The α/β ratio is an indicator of the relative importance of the linear and quadratic terms. Empiric observations suggest that the importance of repair effects usually increases as the α/β ratio decreases. Very recently, the value of α/β for prostate cancer has become a highly debated topic, with evidence demonstrating that α/β may be much lower than that is normally suggested for tumors (18–21). The α/β ratio recently published in the literatures ranges from 1.2 Gy to 3.1 Gy (18–21).

In addition, dose-rate effects in IMRT treatment plans would be expected to make cell killing more nonuniform over the planning target volume than the dose distribution would indicate. Different tumor regions/voxels may experience different dose-time patterns during an IMRT delivery. This difference may result in fairly different BED and may generate cold spots within the target, which, in turn, may diminish the tumor control probability (TCP).

In this study, we have investigated the impact of fraction delivery time on equivalent uniform dose (EUD) and TCP using the LQ formalism. A series of simulated and clinical IMRT plans with different fraction delivery times were evaluated in terms of EUD and TCP using the LQ parameters derived from compiled clinical data for prostate cancer. To study the dependence of EUD and TCP values on model parameters, calculations for a range of radiosensitivity parameters were also carried out. The influence of instantaneous dose-rate, beam-on time, number of segments, and leaf-sequencing pattern was considered in this study. The effects of fraction delivery times in the range of 0 to 45 min on cell killing/tumor control are presented.

METHODS AND MATERIALS

Dose protraction factor in LQ model

The general LQ model, extended to include the effects of dose rate, repair of sublethal damage, and clonogen proliferation (22–24), was used in this study. In this model, the surviving fraction S of cells irradiated to a total dose D within an overall treatment time T is given by

$$S = e^{-E}, \tag{1}$$

$$E = \alpha D + \beta G D^2 - \gamma T, \tag{2}$$

where α and β characterize intrinsic radiosensitivity, G is the dose protraction factor, and γ is the effective tumor-cell repopulation rate [$\gamma = ln\ (2)/T_d$, where T_d is the effective tumor-potential doubling time]. The quantity E is the effective yield of lethal DNA damage per cell (i.e., the yield of lethal DNA damage taking into account repopulation effects).

The dose protraction factor G accounts for sublethal damage repair that occurs during fraction delivery as well as between fractions. The general form for G as a function of treatment time t is (11, 25)

$$G(t) = \frac{2}{D^2}\int_0^t dw I(w)\int_0^w dv I(v) e^{-\mu(w-v)}, \tag{3}$$

where $I(t)$ is the dose-rate function, μ is the repair rate of tumor cells [$\mu = ln(2)/T_r$, where T_r is the repair half-time]. For acute exposure conditions (e.g., high dose-rates), G approaches unity. Conversely, G approaches zero for protracted exposure conditions (i.e., in the limit as the dose rate approaches zero). For the segmented fraction delivery schemes such as IMRT, the temporal pattern of radiation delivery can be modeled as $I(t) = I_i$, $t_{i-1} < t \le t_i$, where $i = 1$ to N, I_i is the dose rate of the ith segment to the voxel in question, and N is the total number of segments for the entire treatment course. Here we treat the time interval between two consecutive segments with nonzero dose also as a segment, with $I = 0$. In this case, G has the following closed-form solution:

$$G = \frac{2}{\mu^2 D^2}\sum_{i=1}^{N} I_i\Big\{ I_i[\mu(t_i - t_{i-1}) - (1 - e^{-\mu(t_i - t_{i-1})})] + \sum_{j=1}^{i-1} I_j(e^{\mu t_j} - e^{\mu t_{j-1}})(e^{-\mu t_{i-1}} - e^{-\mu t_i})\Big\}, \tag{4}$$

where i and j are the summation indices over all dose segments.

Prostate cancer was selected as an example to demonstrate the calculation. Except where explicitly noted otherwise, all of the reported results are based on the LQ parameters of prostate cancer reported by Wang *et al.*: $\alpha = 0.15$ Gy^{-1}, $\alpha/\beta = 3.1$ Gy, $T_r = 16$ min (18). This set of LQ parameters provides realistic estimates of the radiosensitivity and the number of clonogens for prostate cancer (18). The effect of tumor repopulation is ignored in the EUD calculation because we assume the EUD is delivered in similar overall treatment time. In TCP calculations, the effects of tumor repopulation need to be considered even when the growth fraction is small (see discussion in Ref. 18). For prostate cancer, a median potential doubling time of $T_d = 42$ days is used for all of the reported studies (18, 26). For other tumors, the following representative LQ parameters are used for the EUD calculations: $\alpha = 0.4$ Gy^{-1}, $\alpha/\beta = 10$ Gy, $T_r = 20$ min (11, 27).

EUD and TCP

The EUD concept was originally proposed by Niemierko (28) for EBRT. It is defined as the equivalent dose that, if distributed uniformly across the tumor volume, will lead to the same level of cell killing as a nonuniform dose distribution. The EUD provides a means to evaluate the effectiveness of rival IMRT plans. The EUD used in this study is defined relative to an EBRT delivered as a series of 2 Gy fractions ($d = 2$ Gy) (29). A fraction delivery time of 2 min is used for the reference EBRT treatment. For the generalized LQ cell survival model, the EUD is given by (29)

$$EUD = \frac{-\log(S)}{\alpha + \beta d}. \tag{5}$$

To account for dose heterogeneity, the surviving fraction S was calculated based on dose–volume histogram (DVH) by

$$S = \sum_k v_k S(D_k), \tag{6}$$

where v_k is the fractional volume of dose bin D_k in the DVH. The density of tumor clonogens throughout the tumor is presumed constant (see a typical value for prostate tumors at the end of this subsection).

The EUD provides a useful means for comparing the overall effectiveness of rival treatment plans. To help identify potential cold spots in the treatment plan, it is also useful to have a voxel-by-voxel indicator of treatment effectiveness. EUD_i is used to represent the equivalent dose for the ith voxel delivered in the specified method. For a given voxel, the spatial and temporal pattern of radiation delivery should be very nearly the same throughout the entire voxel. A typical voxel size can be as large as a cube of 0.5 cm by 0.5 cm by 0.5 cm.

TCP is often used as an alternate or supplemental indicator of treatment outcome. The often-used Poisson TCP model relates the surviving fraction S to the probability that all tumor cells are eradicated, i.e. (30, 31)

$$TCP = e^{-KS}, \tag{7}$$

where K is the number of tumor clonogens. The intermediate-risk group of prostate cancer was selected as an example of patient groups for analysis. This risk group is defined to possess one and only one of the following presentations: Prostate-specific antigen >10 ng/mL, Gleason score >6, and in stage T2c or higher. All of the studies reported in this work are based on 3.0×10^6 tumor cells, which was found to be appropriate for the intermediate-risk patient group (18).

Impact of fraction delivery time

A typical IMRT treatment plan comprises 5–9 fields (beam orientations) which is typically higher than the number of fields employed in conventional EBRT, and each field contains about 20–40 segments. This results in over 100 total segments for the IMRT plan. When this IMRT is delivered in the step-and-shoot mode, it will take a prolonged time. This is because a period of 0.5–1 min is required to adjust the gantry and couch for each field, and usually, there is also a delay of a few seconds when the MLC leaves move from one segment (defining the previous field shape) to the next segment (defining the next field shape). Furthermore, IMRT treatments must use additional monitor units (MU) (about 10 times as many) than conventional EBRT treatments because of the segmented delivery pattern in which small portions of the tumor are irradiated at any given time. As a result of all the above factors, the total fraction delivery time for IMRT plans may be prolonged to 15–45 min. In comparison, the typical beam-on time and the fraction delivery time for conventional EBRT are approximately 1–2 and 2–5 min, respectively. The beam-on time is defined as the summation of segments that contribute nonzero dose to the voxel of interest.

To help quantify how different aspects of IMRT dose delivery may impact treatment effectiveness, we modeled the temporal pattern of fraction delivery in three stages. First, the EUD and TCP were calculated as a function of total fraction delivery time (simple IMRT dose delivery model). Sensitivity studies were conducted to examine how the predicted EUD and TCP values are affected by intrinsic radiosensitivity (α/β ratio) and the repair half-time for sublethal damage. Second, EUD calculations were performed for a series of simulated IMRT plans. In this series of studies, we examined the effects of the number and distribution of IMRT segments, the beam-on time, and the total fraction delivery time. In a third series of calculations, an IMRT dose distribution for a prostate patient case treated at our institution was used to validate the above calculations.

(1) Simple IMRT fraction delivery model. To study the effects of protracted fraction delivery, we first used a simplified IMRT fraction delivery model. In this simplified

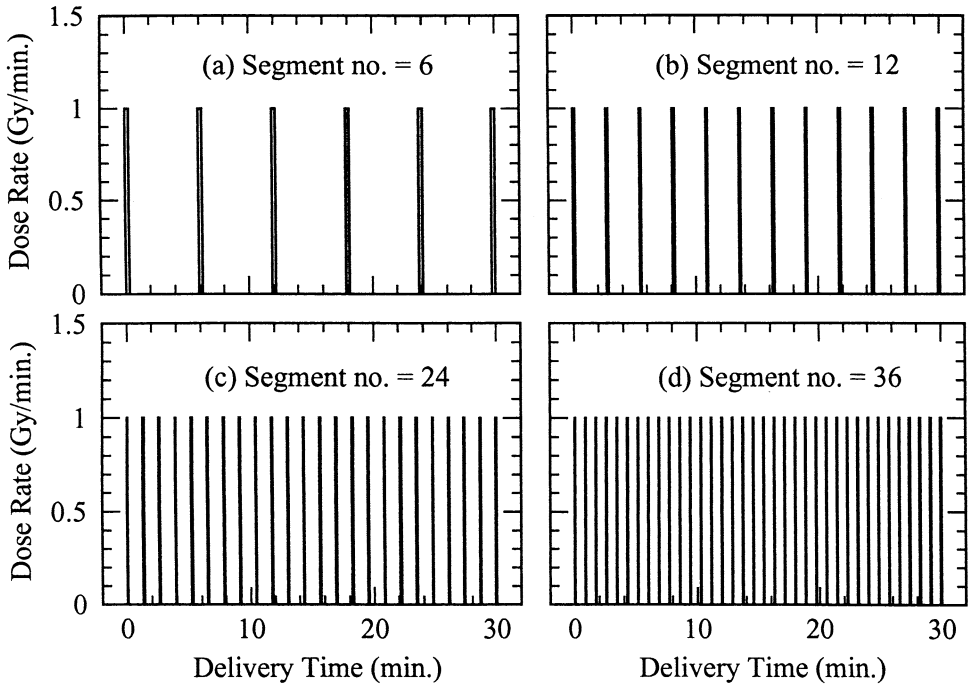

Fig. 1. Four IMRT fraction delivery patterns in a voxel. The 1.8 Gy fractional dose is delivered in 30 min by 6, 12, 24, or 36 segments. Note that the dose per segment varies inversely with the number of total segments. This is represented by the width of the bars in the plots.

IMRT fraction delivery model, each fraction is delivered at constant dose rate I_0 during in time interval t. With this model, we were able to study the cell-killing efficiency as a function of the delivery time t, the tumor α/β ratio, or the repair half-time T_r. The software *AutoEUD* described in a previous paper (29) was used to calculate the EUD and TCP. A representative DVH obtained from conventional EBRT (Fig. 1 of Ref. 29) was used to account for dose inhomogeneity for both conventional EBRT and IMRT plans. It is well known that the 3-D dose distribution generated by IMRT is generally less homogeneous than that of conventional EBRT. A calculation using a typical IMRT DVH instead of the EBRT DVH was performed. The result shows little difference between the EUD and TCP values obtained with the two DVHs. This justifies the use of the single DVH for the rest of the calculations. Calculations were carried out for a prescription dose of 81 Gy with fraction size of 1.8 Gy.

(2) Influence of segment number. In an IMRT plan, a large number of segments are normally used. The number of segments can range from 50 to more than 200. In the above calculation with the simple dose protraction model, the effect of segment numbers was ignored. To take into account this effect, we assume each fraction is divided into n segments with a fixed dose rate of 1 Gy/min for each segment. For simplicity, the n segments are assumed to distribute uniformly within the delivery time t_0. By varying n, we can identify any influence from the segmentation of fractions. Figure 1 shows an IMRT plan of four different segmentation patterns delivering 1.8 Gy per fraction. The number of segments was 6, 12, 24, and 36 respectively. These segments were distributed uniformly within a delivery time of 30 min. The dose per segment varies inversely with the total number of segments. Based on these dose-time patterns, the values of EUD were calculated.

(3) Simulation of IMRT treatment plans. The above calculation considered a fixed dose rate. For a realistic IMRT delivery, the instantaneous dose rate in each voxel is a function of time. That is, the pattern of radiation delivery in each voxel may be very different in both time and space. The fraction delivery time, the number of segments that contribute nonzero dose to the voxel, and the delivered dose to the voxel by each segment may also be quite different. We used the simulations to investigate the potential impact that these phenomena may have on IMRT treatment effectiveness.

For a given voxel, first we randomly pick a number n for the segments with nonzero dose in a range $[N_1, N_2]$, where N_1, N_2 are the lower and upper limits of the number of the nonzero dose segments, respectively. Second, we assign a dose rate I_i for the ith segment according to a uniform dose-rate distribution in $[0.5, 1.5] \times \bar{I}$ (where $\bar{I}$ is the mean dose rate in Gy/min). Third, we determine the duration p_i and the interval q_i (the time interval between the ith and $(i + 1)$th segments) for the ith segment according to Gaussian distributions ($\bar{p} = d_0/(\bar{I} \cdot n)$, $\sigma_p = \bar{p}/2$; $\bar{q} = (t_0 - n\bar{p})/n$, $\sigma_q = \bar{q}/2$, where $\bar{p}$ and σ_p are the mean value and standard deviation of the segment duration respectively, $\bar{q}$ and σ_q are the mean value and standard deviation of the segment intervals respectively, d_0 is the prescribed dose per fraction, and t_0 is the total delivery time for each fraction. Finally, the dose rate is normalized to ensure a total dose of 1.8

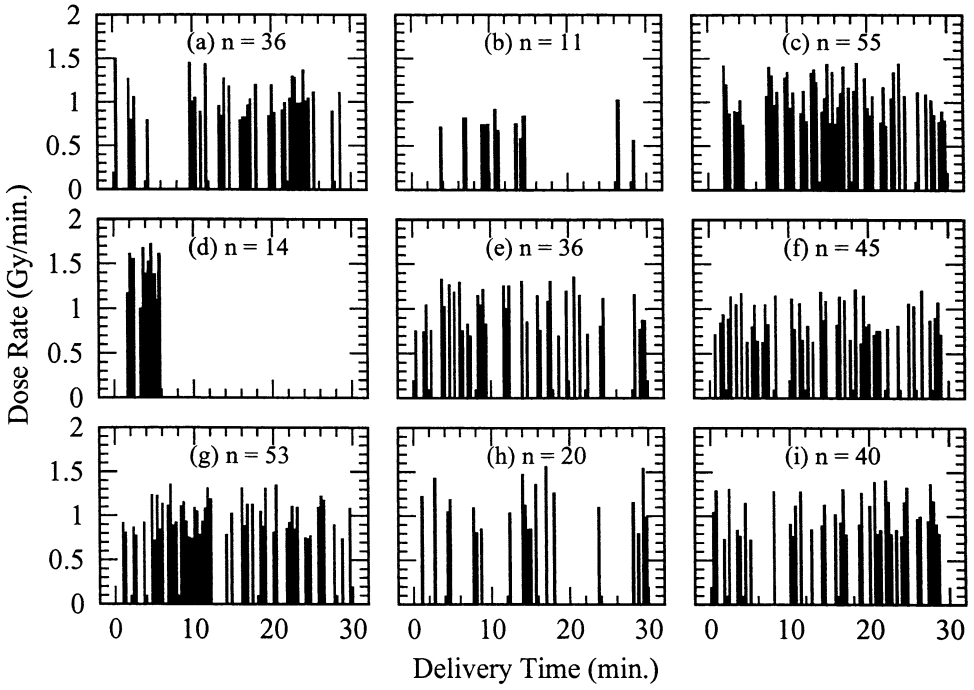

Fig. 2. Simulated segment distributions. Plots (a)–(i) represent the dose-time patterns for nine individual voxels. The variable *n* represents the number of segments that contribute nonzero dose to the voxel. The dose per fraction is 1.8 Gy. The fraction delivery time is 30 min.

Gy delivered for each fraction. The dose-time patterns generated following the above method for 9 voxels are displayed in Fig. 2. The corresponding values of EUD were calculated.

(4) Clinical IMRT plan. A realistic IMRT plan generated for a prostate cancer case was used to study the overall effects identified in the above calculations. The IMRT plan consists of five fields with each field containing 35–45 segments (total 195 segments). The prescription dose was 81 Gy with 1.8 Gy per fraction. The voxel size was 0.5 cm $\times$ 0.5 cm $\times$ 0.3 cm, which was small enough to ensure similar dose-time pattern throughout the entire voxel. A total of 96 voxels within a volume of 2 cm $\times$ 2 cm $\times$ 1.8 cm in part of the target were selected for this calculation. The dose-time distributions in nine randomly selected voxels are presented in Fig. 3. A clear picture of the five fields can be seen from these dose-time patterns.

The distributions of the actual fraction dose delivered, delivery time, and beam-on time for the 96 voxels are shown as histograms in Fig. 4. The fraction dose delivered distributes from 1.6 Gy to 2.0 Gy, with a mean value of 1.8 Gy. The actual fraction delivery time is similar for all 96 voxels (around 27–28 min). The beam-on time is in the range of 2.2 to 3.0 min.

RESULTS

Effects of dose protraction

Figure 5 shows the EUD and TCP values calculated for the simplified IMRT plans as a function of the fraction delivery time. All calculations are based on the generalized LQ parameters for prostate cancer ($\alpha = 0.15$ Gy^{-1}, $\alpha/\beta = 3.1$ Gy, and a 16-min repair half-time) (18). The prescription dose is 81 Gy with fraction size of 1.8 Gy (45 fractions). The intermediate-risk patient group was selected for the TCP calculation. The calculations shown in Fig. 5 clearly demonstrate that both the EUD and TCP decrease with increasing fraction delivery time. When the delivery time increases from 2–5 min (conventional EBRT) to 30 min (typical IMRT), the EUD for prostate cancer decreases from 78 Gy to 69 Gy (a reduction of 12%), and the TCP decreases from 95% to 73%. A reduction in the EUD or TCP of this magnitude may be clinically significant. For a given prescription dose, these predictions suggest that the static IMRT (e.g., step-and-shoot IMRT), as currently practiced, is less effective at local tumor control than conventional EBRT or dynamic IMRT. The prescription dose for static IMRT (either dose per fraction or the number of fractions) may need to be higher than the prescription dose for either conventional EBRT or dynamic IMRT to account for their differences in fraction delivery times. For prostate cancer, the total dose may need to be escalated by as much as 5 to 12 Gy (for 15 to 45 min fraction delivery times), as demonstrated in Fig. 5.

Figure 6 shows how the calculated EUD depends on intrinsic radiosensitivity (α/β ratio) and the repair half-time T_r. The dashed and solid curves are for delivery times of 2 and 30 min, respectively. The EUD is very sensitive to the α/β ratio. A lower α/β ratio, such as 1.5 Gy reported for prostate cancer by several investigators (19–21), leads to an even lower EUD (64 Gy) for a 30-min delivery time. The

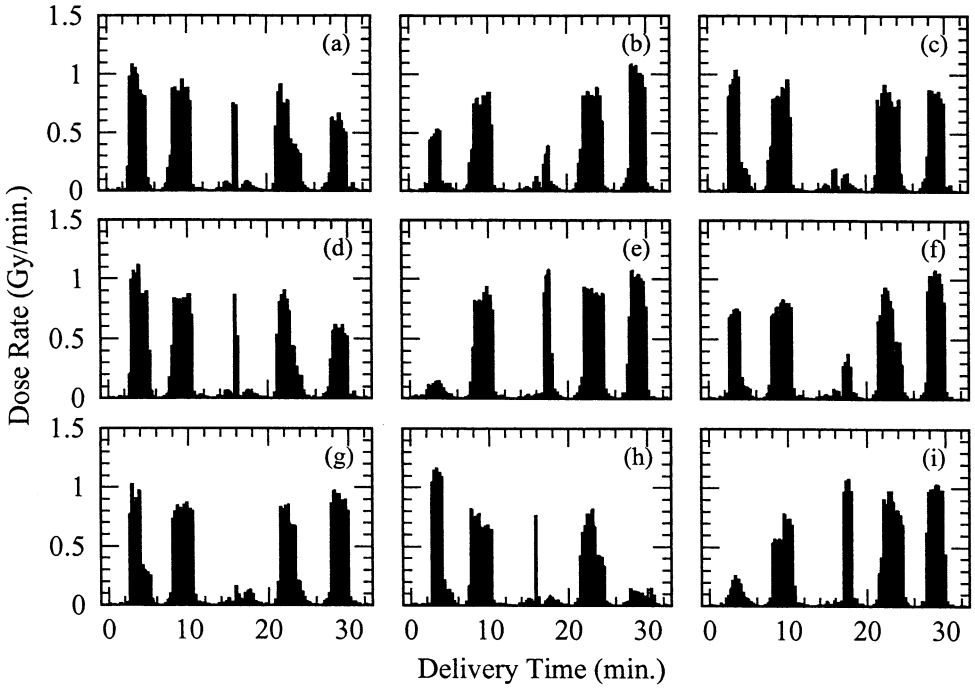

Fig. 3. Clinical IMRT plan: dose-time patterns in nine individual voxels [plots (a)–(i)] within the target for a prostate patient case. The fraction of 1.8 Gy was delivered with a delivery time of 33 min.

effects of the delivery time decrease as the α/β ratio or the repair half-time of sublethal damage increases. For an IMRT with a delivery time of 45 min, the EUD is reduced by 3.5 Gy as compared to the conventional EBRT treatment even if the half-time for repair is 1 h. For such a situation, a dose escalation of about 3.5 Gy may be needed to compensate for the dose protraction effect.

Figure 7 shows the EUD calculation using the LQ parameters that are often considered typical for many tumors (i.e., $\alpha = 0.4\ \text{Gy}^{-1}$, $\alpha/\beta = 10$ Gy, $T_r = 20$ min) (11, 27). Because the α/β ratio is large, the influence of dose protraction is small. However, the results shown in Fig. 7 suggest that an additional 2 to 4 Gy overall may still be needed to correct the dose protraction effect. When the repair half-time increases over 1 h, this dose protraction effect becomes negligible.

Influence of segment number

EUD was calculated for simulated IMRT prostate plans with varying number of segments. Figure 8 shows the EUD values as a function of the number of segments with the same overall fraction delivery time. A prescription dose of 81 Gy and a fraction size of 1.8 Gy were assumed. The delivery time was assumed to be 30 min. The EUD quickly approaches an asymptotic value of 68.3 Gy when the number of segments becomes larger than 10. This EUD value is consistent with the general results presented in Fig. 5. These calculations suggest that, for a given IMRT fraction delivery

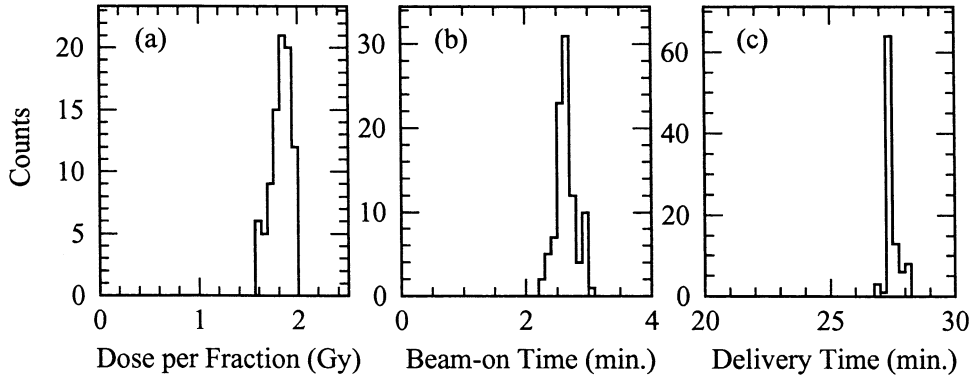

Fig. 4. Clinical IMRT plan: histograms of (a) delivered dose, (b) beam-on time, and (c) delivery time per fraction for 96 voxels within the prostate target.

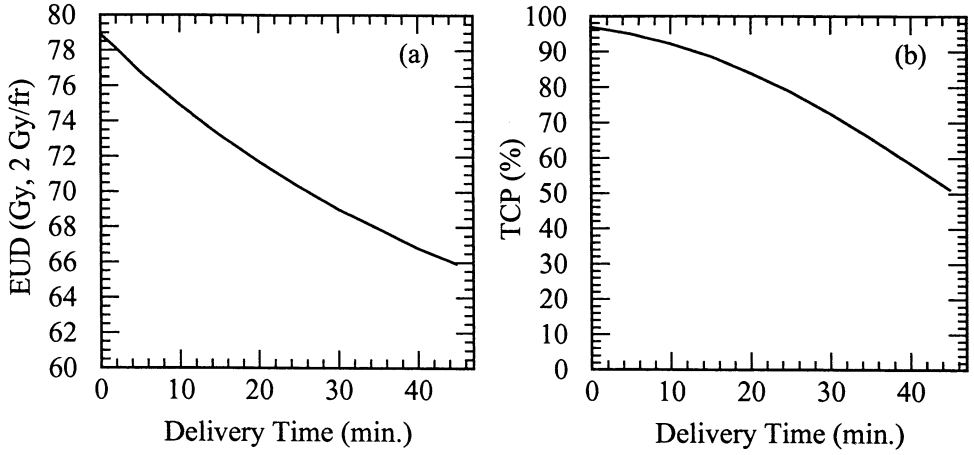

Fig. 5. (a) Equivalent uniform dose (EUD) and (b) tumor control probability (TCP) for an intermediate-risk patient group as a function of IMRT fraction delivery time for prostate cancer. The prescription dose is 81 Gy in 1.8 Gy fractions. Except where explicitly noted otherwise, the following LQ parameters were used in this study: $\alpha = 0.15$ Gy^{-1}, $\alpha/\beta = 3.1$ Gy, $T_r = 16$ min, and clonogen number $K = 3.0 \times 10^6$ (18).

time, the number of segments has little impact on cell killing. The present observation on the effect of segment number is similar to that observed in animal experiments using pulsed-dose-rate (PDR) brachytherapy. Armour *et al.* (32) have reported that for late rat rectal injury, there is no distinguishable difference among dose responses in various PDR with pulse sizes up to 1.5 Gy.

Simulation of IMRT

Following the simulation procedure described in the "Methods and Materials" section, we have generated dose-time distributions for 1000 voxels. The dose-time pattern in each voxel was similar to those presented in Fig. 2. A time of 30 min was assumed for the fraction delivery, but the actual fraction delivery time might vary from voxel to voxel. The EUD calculations are based on a prescription dose of 81 Gy (1.8 Gy fractions). Figure 9 shows a scatter plot of EUD values in these 1000 voxels vs. the delivery time. The mean EUD in voxel is approximately 69 Gy with a standard deviation of 0.6 Gy. This figure clearly indicates that the EUD for a given voxel is mainly determined by the fraction delivery time for the voxel. The EUD is almost independent of the instantaneous dose rate, the beam-on time, and the number, size, and distribution of segments.

Clinical IMRT plan

Similar analysis has been performed for the clinical IMRT prostate case. The EUD values for the selected 96 voxels in the target were calculated. Figure 10 shows the scatter plots of these EUDs vs. the delivered dose per fraction. Results are shown for all 96 voxels. Because the

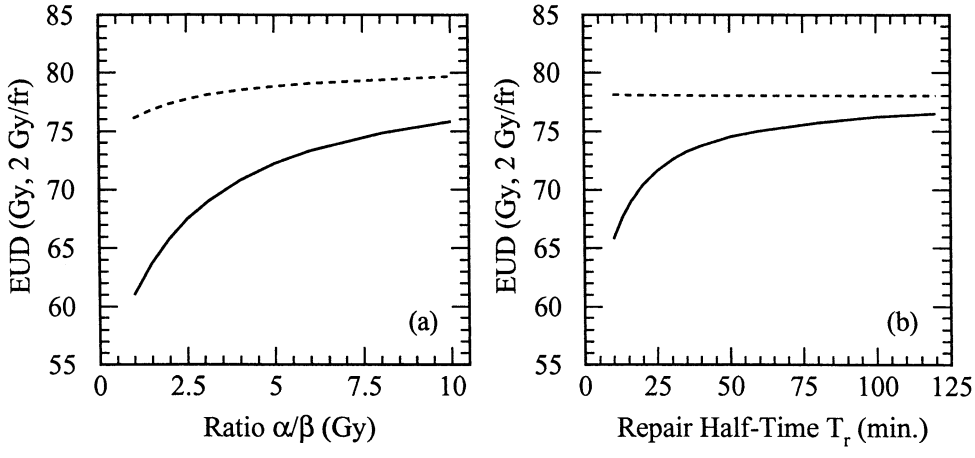

Fig. 6. EUD as a function of (a) α/β ratio and (b) repair half-time T_r for prostate cancer. The prescription dose is 81 Gy in 1.8 Gy fractions. The LQ parameters of Wang *et al.* (18) were used except for the α/β ratio in plot (a) and the repair half-time T_r in plot (b), where they are free parameters, respectively. The fraction delivery time is 2 min (dashed curve) and 30 min (solid curve), respectively.

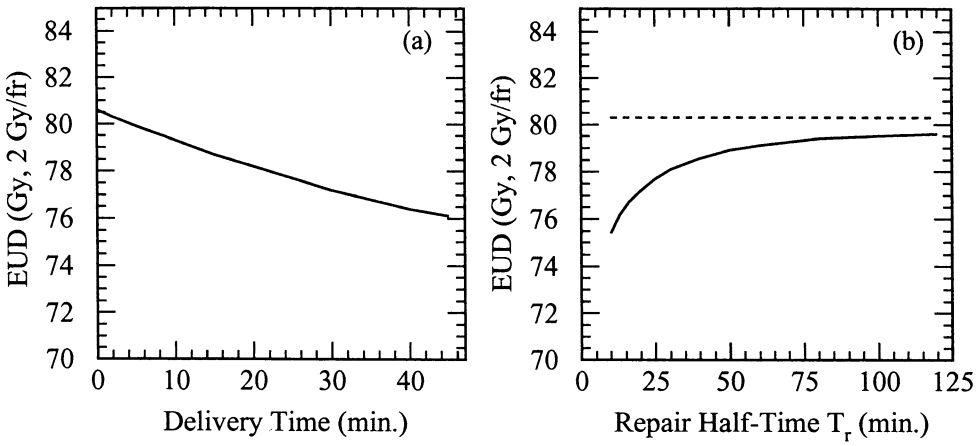

Fig. 7. EUD as a function of (a) fraction delivery time and (b) repair half-time T_r for typical tumors. The prescription dose is 81 Gy in 1.8 Gy fractions. The LQ parameters used are as follows: $\alpha = 0.4$ Gy^{-1}, $\alpha/\beta = 10$ Gy, $T_r = 20$ min (11, 27). In plot (b), the repair half-time T_r is a free parameter. The fraction delivery time is 2 min (dashed curve) and 30 min (solid curve) respectively.

delivery time is approximately 28 min for most voxels, the EUD for voxels with 1.8 Gy fraction dose is about 68.5 Gy regardless of any differences in the dose-time patterns among these voxels. Again it is consistent with the general results shown in Fig. 5. The calculations for this clinical case provide additional support for the hypothesis that fraction delivery times may impact EUD and TCP. Given the same overall fraction delivery time, the effects of instantaneous dose rate, beam-on time, and the number, size, and distribution of segments can be reasonably neglected in IMRT treatment planning.

CONCLUSIONS AND DISCUSSION

The potential impact that fraction delivery time has on local tumor control has been studied using the LQ formalism and the radiosensitivity parameters derived from clinical data for prostate cancer. The modeling studies predict that the time to deliver a fraction using static IMRT may decrease the EUD and TCP. Tumors with a low α/β ratio and a short half-time for sublethal damage repair, such as prostate cancer, will likely be more sensitive to fraction delivery time than tumors with larger α/β ratios and/or longer repair half-times. These effects, if confirmed by clinical studies, should be considered in designing IMRT plans.

Several different approaches could be used to negate the decreases in tumor-cell killing associated with increasing fraction delivery times. For example, if technology permits, one could use dynamic, instead of static (step-and-shoot) IMRT to shorten the fraction delivery time. Dynamic IMRT has been shown to result in 2–2.5 times less total delivery time compared with static IMRT (33). An example of dynamic IMRT is intensity-modulated arc therapy (IMAT). It has been shown that a typical IMAT treatment can be delivered in equal or less time as compared with conventional treatments (34, 35).

Another way to reduce IMRT delivery time is to optimize

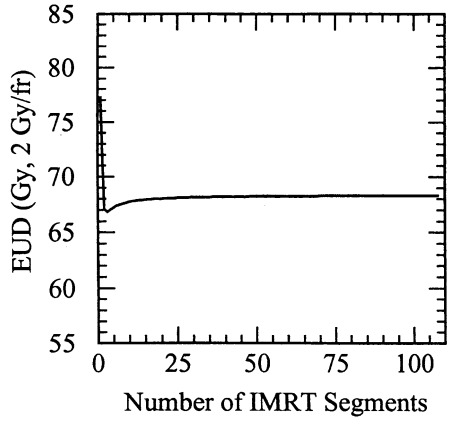

Fig. 8. EUD vs. the number of IMRT segments for prostate cancer. The prescription dose is 81 Gy in 1.8 Gy fractions. The fraction delivery time is 30 min.

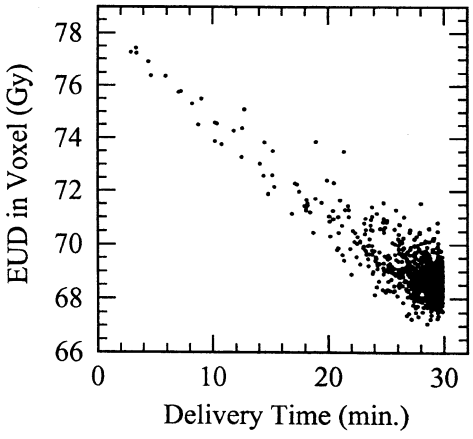

Fig. 9. Scatter plots of EUD in voxel vs. delivery time per fraction for 1000 voxels simulated. The prescription dose is 81 Gy in 1.8 Gy fractions.

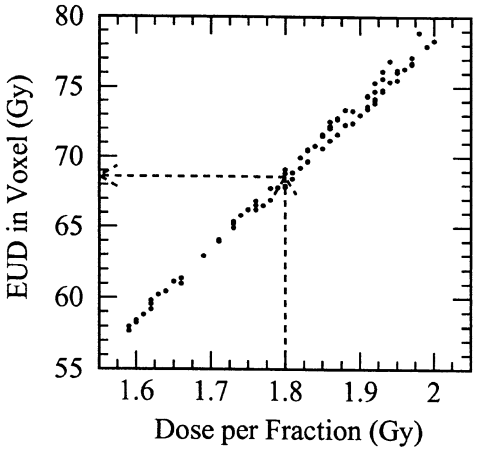

Fig. 10. Scatter plots of EUD in voxel vs. delivered dose per fraction for 96 voxels of clinical IMRT plan. The dashed arrows show the EUD for voxels with the prescribed dose of 1.8 Gy per fraction. The prescription dose is 81 Gy in 1.8 Gy fractions. The delivery time is approximately 28 min for each individual voxel.

the leaf sequencing and reduce the number of segments (3, 36, 37). New inverse planning algorithms that use fewer segments while not sacrificing too much on dose uniformity and conformity are being developed (36, 37). An example of such algorithms is the direct aperture optimization (DAO) method. The IMRT plans generated by DAO can be delivered within 10 min using step-and-shoot technology (37).

Our results suggest that if IMRT with a delivery time longer than 10–15 min is employed, the prescription dose may have to be increased to compensate for the reduction in cell killing due to the increased sublethal damage repair. The prescription dose can be escalated by increasing fractional dose and/or by increasing the number of fractions.

It has been argued that hypofractionation may be preferred for tumors with low α/β ratio (38). Increased effectiveness of hypofractionation for prostate cancer has been shown in a calculation based on radiosensitivity parameters derived from clinical data (29). A clinical study on hypofractionated IMRT that delivers 70 Gy at 2.5 Gy per fraction has shown a comparable biochemical relapse profile with the three-dimensional conformal radiotherapy of 78 Gy in 2.0 Gy fractions, but with more favorable late rectal toxicity profile (39). The IMRT dose was delivered using a dynamic MLC in this study.

The present study focuses on local tumor control. In contrast to tumor control, the prolonged fraction delivery time may have a positive impact on normal tissue sparing because more time is available for sublethal damage repair. There is clinical evidence and *in vitro* data (40–43) showing that the normal tissues, such as rectum, may possess a much longer repair half-time than tumor cells. Therefore, the fraction delivery time should have less impact on the normal tissue based on this study. With the improved normal tissue sparing of IMRT, it may be possible to substantially improve the overall treatment outcome by reducing the fraction delivery time.

The results generated in this study may be limited by the approximations used in the models and by the lack of more reliable model parameters. Dose inhomogeneity was considered with a representative DVH for both conventional EBRT and IMRT. Both intra- and intertumor variations were ignored. Caution needs to be exercised in using the presented data for clinical decision-making purpose.

REFERENCES

1. Bortfield TR, Kahler DL, Waldron TJ, *et al.* X-ray field compensation with multileaf collimators. *Int J Radiat Oncol Biol Phys* 1994;28:723–730.
2. Brahme A. Optimization of radiation therapy. *Int J Radiat Oncol Biol Phys* 1994;28:785–787.
3. Siochi RA. Minimizing static intensity modulation time using an intensity solid paradigm. *Int J Radiat Oncol Biol Phys* 1999;43:671–680.
4. Webb S. Intensity-modulated radiation therapy. Bristol, UK: Institute of Physics Publishing; 2001. p. 1–19, 75–96.
5. Galvin JM, Chen XG, Smith RM. Combining multileaf fields to modulate fluence distribution. *Int J Radiat Oncol Biol Phys* 1993;27:697–705.
6. Stewart RD, Traub RJ. Radiobiological modeling in voxel constructs. In: Kling A, Barão F, Nakagawa M, *et al.*, eds. The MC2000, an international conference on advanced Monte Carlo for radiation physics, particle transport simulation and applications. New York: Springer-Verlag; 2001. p. 285–290.
7. Stewart RD, Traub RJ. Temporal optimization of radiotherapy treatment fractions. In: Proceedings of the ANS Topical Meeting on Radiation Protection for our National Priorities, Medicine, the Environment, and the Legacy (RPS 2000). La Grange Park, IL: American Nuclear Society; 2000. p. 372–378.
8. Deasy JO, Fowler JF, Roti JL, *et al.* Dose-rate effects in intensity modulated radiation therapy (abstr). *Int J Radiat Oncol Biol Phys* 1997;51:400–401.
9. Morgan WF, Naqvi SA, Yu C, *et al.* Does the time required to deliver IMRT reduce its biological effectiveness? (abstr). *Int J Radiat Oncol Biol Phys* 2002;54:222.
10. Steel GG, Deacon JM, Duchesne GM, *et al.* The dose-rate effect in human tumour cells. *Radiother Oncol* 1987;9:299–310.
11. Brenner DJ, Hall EJ. Conditions for the equivalence of continuous to pulsed low dose rate brachytherapy. *Int J Radiat Oncol Biol Phys* 1991;20:181–190.
12. Kampinga HH, Hiemstra YS, Konings AWT, *et al.* Correlation between slowly repairable double-strand breaks and thermal radiosensitization in the human HeLa S3 cell line. *Int J Radiat Biol* 1997;72:293–301.
13. Ang KK, Jiang GL, Guttenberger R, *et al.* Impact of spinal cord repair kinetics on the practice of altered fractionation schedules. *Radiother Oncol* 1992;25:287–294.
14. Millar WT, Canney PA. Derivation and application of equations describing the effects of fractionated protracted irradiation, based on multiple and incomplete repair processes. Part 2. Analysis of mouse lung data. *Int J Radiat Biol* 1993;64: 293–303.
15. Van Rongen E, Thames HD, Jr, Travis EL. Recovery from radiation damage in mouse lung: Interpretation in terms of two repair rates. *Radiat Res* 1993;133:225–233.

16. Stewart RD. Two-lesion kinetic model of DSB rejoining and cell killing. *Radiat Res* 2001;156:365–378.
17. Guerrero M, Stewart RD, Wang JZ, Li XA. Equivalence of the linear-quadratic and two-lesion kinetic models. *Phys Med Biol* 2002;47:3197–3209.
18. Wang JZ, Guerrero M, Li XA. How low is the α/β ratio for prostate cancer? *Int J Radiat Oncol Biol Phys* 2003;55:194–203.
19. Brenner DJ, Hall EJ. Fractionation and protraction for radiotherapy of prostate carcinoma. *Int J Radiat Oncol Biol Phys* 1999;43:1095–1101.
20. Fowler JF, Chappell RJ, Ritter MA. Is α/β for prostate cancer really low? *Int J Radiat Oncol Biol Phys* 2001;50:1021–1031.
21. Brenner DJ, Martinez AA, Edmundson GK, *et al.* Direct evidence that prostate tumors show high sensitivity to fractionation (low α/β ratio), similar to late-responding normal tissue. *Int J Radiat Oncol Biol Phys* 2002;52:6–13.
22. Thames HD. An incomplete-repair model for survival after fractionated and continuous irradiations. *Int J Radiat Biol* 1985;47:319–339.
23. Dale RG. The application of the linear-quadratic dose-effect equation to fractionated and protracted radiotherapy. *Br J Radiol* 1985;58:515–528.
24. Dale RG. Radiobiological assessment of permanent implants using tumor repopulation factors in linear-quadratic model. *Br J Radiol* 1989;62:241–244.
25. Manning MA, Zwicker RD, Arthur DW, *et al.* Biologic treatment planning for high-dose-rate brachytherapy. *Int J Radiat Oncol Biol Phys* 2001;49:839–845.
26. Haustermans K, Fowler JF. A comment on proliferation rates in human prostate cancer [letter to editor]. *Int J Radiat Oncol Biol Phys* 2000;48:303.
27. Thames HD, Bentzen SM, Turesson I, *et al.* Time-dose factors in radiotherapy: A review of the human data. *Radiother Oncol* 1990;19:219–235.
28. Niemierko A. Reporting and analyzing dose distribution: A concept of equivalent uniform dose. *Med Phys* 1997;24:103–110.
29. Wang JZ, Li XA. Evaluation of external beam radiotherapy and brachytherapy for localized prostate cancer using equivalent uniform dose. *Med Phys* 2003;30:34–40.
30. Webb S, Nahum AE. A model for calculating tumor control probability in radiotherapy including the effects of inhomogeneous distributions of dose and clonogenic cell density. *Phys Med Biol* 1993;38:653–666.
31. Webb S. Converting 3D dose to biological outcomes: Tumor control probabilities (TCP) and normal tissue complication probabilities (NTCP). In: Mould RF, Orton CG, Spaan JAE, *et al.*, eds. The physics of conformal radiotherapy. Advances in technology. Bristol, UK: Institute of Physics Publishing; 1997. p. 258–287.
32. Armour EP, White JR, Armin A, *et al.* Pulsed low dose rate brachytherapy in a rat model: Dependence of late rectal injury on radiation pulse size. *Int J Radiat Oncol Biol Phys* 1997; 38:825–834.
33. Chui CS, Chan MF, Yorke E. Delivery of intensity-modulated radiation therapy with a conventional multileaf collimator: Comparison of dynamic and segmental methods. *Med Phys* 2001;28:2441–2449.
34. Li XA, Ma L, Naqvi S, *et al.* Monte Carlo dose verification for intensity modulated arc therapy. *Phys Med Biol* 2001;46: 2269–2282.
35. Yu CX, Li XA, Ma L, *et al.* Clinical implementation of intensity-modulated arc therapy. *Int J Radiat Oncol Biol Phys* 2002;53:453–463.
36. Crooks SM, McAven LF, Robinson DF, *et al.* Minimizing delivery time and monitor unites in static IMRT by leaf-sequencing. *Phys Med Biol* 2002;47:3105–3116.
37. Shepard DM, Earl MA, Li XA, *et al.* Direct aperture optimization: A turnkey solution for step-and-shoot IMRT. *Med Phys* 2002;29:1007–1018.
38. Fowler JF, Chappell RJ, Ritter MA. The prospects for new treatments for prostate cancer. *Int J Radiat Oncol Biol Phys* 2002;52:3–5.
39. Kupelian PA, Reddy CA, Carlson TP, *et al.* Preliminary observations on biochemical relapse-free survival rates after short-course intensity-modulated radiotherapy (70 Gy at 2.5 Gy/fraction) for localized prostate cancer. *Int J Radiat Oncol Biol Phys* 2002;53:904–912.
40. Cox JD, Pajak TF, Marcial VA, *et al.* Interfraction interval is a major determinant of late effects, with hyperfractionated radiation therapy of carcinomas of upper respiratory and digestive tracts: Results from Radiation Therapy Oncology Group protocol 8313. *Int J Radiat Oncol Biol Phys* 1991;20: 1191–1195.
41. Amdur RJ, Bedford JS. Dose-rate effects between 0.3 and 30 Gy/h in a normal and a malignant human cell line. *Int J Radiat Oncol Biol Phys* 1994;30:83–90.
42. Hall EJ, Brenner DJ. Sublethal damage repair rates—a new tool for improving therapeutic ratios. *Int J Radiat Oncol Biol Phys* 1994;30:241–242.
43. Brenner D, Armour E, Corry P, *et al.* Sublethal damage repair times for a late-responding tissue relevant to brachytherapy (and external-beam radiotherapy): Implications for new brachytherapy protocols. *Int J Radiat Oncol Biol Phys* 1998; 41:135–138.